

Cell Library Characterization for Composite Current Source Models Based on Gaussian Process Regression and Active Learning

Tao Bai^{1,2*}, Junzhuo Zhou^{3*}, Zeyuan Deng^{1,2}, Ting-Jung Lin⁴, Wei Xing⁵, Peng Cao^{1,2†}, Lei He³

¹ National ASIC System Engineering Technology Research Center, Southeast University, Nanjing, China

² National Center of Technology Innovation for EDA, Nanjing, China

³ University of California, Los Angeles, United States

⁴ Ningbo Institute of Digital Twin, Eastern Institute of Technology, Ningbo, China

⁵ The University of Sheffield, Sheffield, United Kingdom

caopeng@seu.edu.cn, lhe@ee.ucla.edu

ABSTRACT

The composite current source (CCS) model has been adopted as an advanced timing model that represents the current behavior of cells for improved accuracy and better capability than traditional non-linear delay models (NLDM) to model complex dynamic effects and interactions under advanced process nodes. However, the high accuracy requirement, large amount of data and extensive simulation cost pose severe challenges to CCS characterization. To address these challenges, we introduce a novel Gaussian Process Regression (GPR) model with active learning (AL) to establish the characterization framework efficiently and accurately. Our approach significantly outperforms conventional commercial tools as well as learning based approaches by achieving an average absolute error of 2.05 ps and a relative error of 2.27% for current waveform of 57 cells under 9 process, voltage, temperature (PVT) corners with TSMC 22nm process. Additionally, our model drastically reduces the runtime to 27% and the storage by up to 19.5× compared with that required by commercial tools.

KEYWORDS

Standard Cell, Current Source Models, Gaussian Process Regression, Active Learning

1 INTRODUCTION

Standard cell libraries are essential in integrated circuit design for performance, power, and area (PPA) optimization, which are characterized to enable accurate timing and power analysis during logical synthesis and physical implementation [1]. Different from traditional non-linear delay models (NLDM) using simple delay values to represent the cell behavior, the composite current source (CCS) model is an advanced timing model that represents the current behavior of cells for improved accuracy and better capability to model complex dynamic effects and interactions under advanced process nodes [2]. However, suffering from considerably increased complexity with advanced nodes, the more time-consuming and resource-intensive computational effort is induced as well as dramatically increased storage requirements [3, 4], which poses a significant challenge for the characterization and timing analysis of CCS model.

The CCS model is composed of three main components, including the receiver model, the driver model, and the reduced-order network model [5]. The driver model represents the behavior of the output driver of a cell, capturing how it generates currents over time in response to input signals, while the receiver model characterizes how the input of a cell responds to incoming signals, focusing on the input pin's electrical characteristics. The reduced-order network model simplifies the complex interconnect network between drivers and receivers, making the CCS model more manageable without losing significant accuracy. Among them, the driver model's accuracy directly impacts the overall timing and noise analysis of the cell, which involves numerous SPICE simulations to generate the current vs. time data for different process, voltage, and temperature (PVT) corners. Inaccurate driver characterization can lead to incorrect predictions of signal behavior, affecting the reliability of the design.

The increasing complexity of semiconductor technology and the number of required PVT corners have introduced severe challenges in CCS characterization due to the high accuracy requirement, large volume of data, and extensive simulation overhead [6]. First, capturing detailed current waveforms requires high-precision measurements and simulations to accurately reflect the dynamic behavior of the driver during switching. Any inaccuracies in these waveforms can lead to incorrect timing and noise predictions [7]. Second, since the characterization must be performed across a wide range of input transition times, output loads, and PVT corners, the amount of data is exponentially increased for current waveforms with high temporal resolution for each cell and each condition. Prior works have been presented to reduce the storage cost by waveform compression, but they focus on the current waveform of single cell only and neglect the correlation among different cell driver strengths and different PVT corners [4, 8]. Third, the sophisticated characterization scenarios also result in time-consuming simulation costs to capture fine-grained current waveforms, potentially slowing down the design cycle. In spite of considerable researches focused on accelerating the characterization of statistical and aging-aware timing libraries [9–12], few of them were devoted into the area of CCS characterization.

To tackle the aforementioned challenges, an accurate and efficient standard cell library characterization framework is proposed in this work for CCS model based on Gaussian Process Regression (GPR) and active learning (AL), which significantly reduces the

*Both authors contributed equally to this research.

†Peng Cao is the corresponding author.

data storage requirement and simulation cost with considerable accuracy for multiple PVT corners and cells with varying driving strengths. The main contributions of this work are summarized as follows.

- To the best of our knowledge, this is the first work to propose a CCS model characterization framework for standard cell library with GPR and AL, which formulates the detailed modeling of current waveform as the uncertainty quantification (UQ) problem and predicts the individual current and time value with high precision and efficiency.
- Considering the uncertainty inconsistency issue, multiple GPR models are employed to improve the prediction precision of the corresponding current points, where the correlation among PVT corners and driving strengths are captured as features to enhance generalization performance and reduce simulation cost.
- The strategy for selecting training data efficiently is implemented by AL, where the samples with the lower contribution to accuracy are selected by UQ and used to retrain GPR models so as to minimize the amount of required training data and accelerate model convergence.

The rest of the paper is organized as follows. Section 2 introduces the related works of standard cell characterization and preliminaries about GPR and AL, and Section 3 introduces the proposed algorithm, and Section 4 discusses our experimental setup and results, followed by conclusion in Section 5.

2 RELATED WORKS AND PRELIMINARIES

2.1 Related Works

In order to improve accuracy, efficiency, and scalability in the characterization process of standard cell library, plenty of studies have been dedicated to developing modeling methodologies for modern process nodes, leveraging machine learning methods, especially supervised learning, to accelerate the establishment of standard cell libraries has become a prominent focus of research.

The deep neural network (DNN) model is applied to perform standard cell characterization for nominal timing [10] and statistical timing [9], respectively, which use data from sparse characterization to generate delay models at required sign-off corners but ignore the relation with transistor-level cell topology. A characterization approach using ridge regression for aging-aware cell library is detailed in [11], which enables designers to assess their circuits under precisely selected degradation scenarios. Similarly, the work of [13] introduced an innovative logical circuit simulation method implemented using neural networks based on the current source model. The research in [14] employs a multi-layer perceptron (MLP) model to create power supply noise (PSN) waveform for each standard cell. Furthermore, [15] utilizes GPR with AL to estimate statistical timing distributions in OCV characterization.

Although various ML algorithms have been utilized, the method for selecting training data of CCS characterization has not been thoroughly studied. This oversight has a significant impact on prediction accuracy and the simulation cost required to generate the data. Moreover, the uncertainty of predicted results by ML algorithms may degrade the accuracy of cell library, which is vital for circuit design.

2.2 Gaussian Process Regression

From a functional space perspective, a Gaussian process (GP) is defined to describe the distribution of functions, enabling direct Bayesian inference within the function space. A GP is a collection where any finite set of random variables possesses a joint Gaussian distribution. The characteristics of a GP are entirely determined by its mean function, $\mu(x)$, and covariance function, $k(x, x')$, as shown in Eq. 1 and 2 [16].

$$\mu(x) = E[f(x)] \quad (1)$$

$$k(x, x') = E[(f(x) - \mu(x))(f(x') - \mu(x')))] \quad (2)$$

where $x, x' \in \mathbb{R}^d$ are arbitrary random variables. The kernel function $k(x, x')$ encapsulates the relationship between the function values at points x and x' . Therefore, the GP can be defined as $f(x) \sim \text{GP}(\mu(x), k(x, x'))$.

GPR model provides an estimate of uncertainty in predictions by quantifying the reliability of the predictions through confidence intervals. In this work, we utilize multiple GPR models to obtain the uncertainty associated with each output.

2.3 Active Learning

Active Learning (AL) strategies in supervised learning allow the training algorithm to "ask questions" by selecting feature vectors to query for their target values during training, usually based on the current model. The primary goal of AL is to reduce the number of training samples needed to achieve a model with high predictive quality, which is especially valuable when obtaining target values is costly or time-consuming, such as requiring human labeling, expensive experiments, or complex simulations. AL methods are usually categorized in query synthesis (or population-based) methods, in which the feature vector to query can be chosen arbitrarily, and pool-based sampling methods, in which the vector can only be chosen within a given finite set (or "pool") of unlabeled values, and selective-sampling methods, in which vectors are proposed in a streaming flow and the AL algorithm can only decide online whether to ask for the corresponding target or not.

Several approaches to AL are available in the literature. Most of the literature focuses on classification problems [17], although AL has been investigated also for regression [18]. In this work, the uncertainty of each output is obtained through the surrogate model. From this, the uncertainty of the sample is derived, allowing for the selection of samples that require labeling.

3 CCS TIMING MODEL CHARACTERIZATION FRAMEWORK

3.1 Problem Formulation

In this work, the accurate CCS model characterization for each specific function of cells, e.g. NAND cell, is formulated as a UQ problem, whose current waveform is represented under N different conditions as $X = x_i | i = 1, 2, \dots, N$. By exploiting the correlation among multiple PVT corners and different driving strengths, the N conditions for a cell include the combinations for timing arc, input transition and output load. With the predicted and real current waveform, the corresponding voltage waveforms could be represented as $V^{(i)}$ and $V^{(i)*}$, whose difference is used to evaluate the

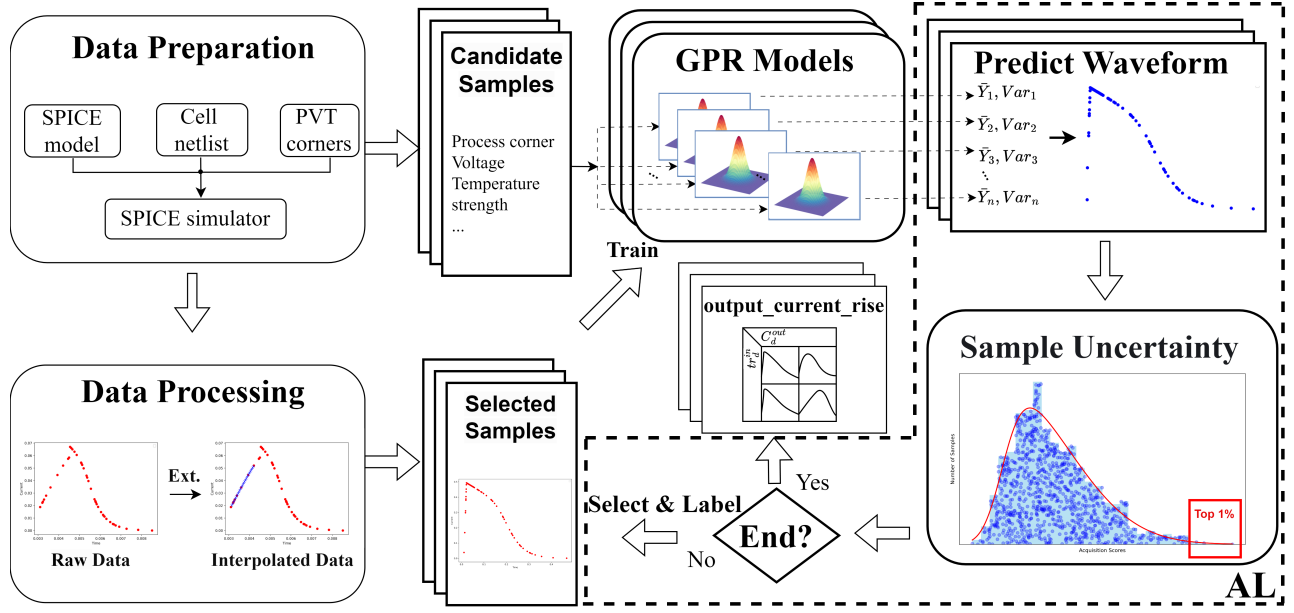


Figure 1: Overview of Proposed Standard Cell Characterization Framework for CCS Model Based on GPR and AL

uncertainty of the characterization framework in terms of root mean squared error (RMSE) as shown in follows.

$$L^{(i)} = \text{RMSE}(V^{(i)} - V^{(i)*}) \quad (3)$$

Therefore, the objective to maximize the accuracy of voltage waveform for CCS model characterization is formulated as the minimization of $L^{(i)}$.

$$\text{Objective: } \min(L^{(i)}) \quad (4)$$

3.2 Overview

Fig. 1 demonstrates the overview of the proposed standard cell characterization framework for CCS model based on GPR and AL. As illustrated in Fig. 1, the SPICE model and cell netlist, as well as the information of PVT corners are prepared for SPICE simulation to generate current waveforms as training data. Considering the different number of current points for specific functions of cells with different driving strengths, linear interpolation operation is performed to extend the original current points to a fixed identical number. For the task of characterization framework establishment for CCS model, the GPR models are trained and AL with processed training data for selected samples and predict the current waveform for candidate samples with the extracted features according to PVT corner and cell netlist. During training, based on the predicted waveform for candidate samples, those with the worst uncertainty, e.g. top 1%, are added into the selected samples to retrain the GPR models repeatedly until the termination criteria are met. Finally, the GPR models are stored as the characterization framework for CCS model to represent the current waveform of each specific function of cells.

3.3 Design of an Algorithm Using GPR with AL

In this section, we detail a comprehensive algorithmic framework designed for the advanced characterization of standard cells. This framework employs GPR models with AL, structured into a series of systematic steps to ensure robust and precise outcomes. Starting with the initialization and training phases, the process flows through a cycle of prediction, evaluation, and iterative refinement, crucial for handling the dynamic complexities of semiconductor data.

3.3.1 Initialization. In this study, we generate standard cell libraries under various Process, Voltage, and Temperature (PVT) corners and different drive strengths. To maintain consistency across the data set, we extend all data to the same length through linear interpolation without compromising the accuracy of the timing information. We then generate a large set of candidate samples, denoted as $X_c = x_i | i = 1, 2, \dots, N$. From this set, we select a subset $X = x_j | j = 1, 2, \dots, M$ with $M < N$, where the associated simulated waveform data, $\mathcal{Y} = y_j | j = 1, 2, \dots, M$, originates from HSPICE simulations. Finally, we normalize the selected samples to facilitate further analysis and modeling.

3.3.2 Gaussian Process Model Training. Using the selected samples X and their corresponding waveform data \mathcal{Y} , we train GPR models to effectively predict and analyze the behavior of standard cells under various conditions.

3.3.3 Waveform Prediction by Gaussian Process Model. We use the trained Gaussian process model to predict the current waveform, leveraging the sophisticated statistical techniques embedded in the model to generate precise waveform outputs from the selected sample data.

3.3.4 Uncertainty Evaluation. The uncertainty of all candidate samples is evaluated using an acquisition function $A^{(i)}$, $i < N$. This acquisition function, which is detailed in Section 3.4, helps quantify the uncertainty associated with each sample's prediction, facilitating more informed decision-making in subsequent steps.

3.3.5 Termination Check. The algorithm performs a termination check to decide whether to continue or stop. If the specified stopping criterion is met, either because the iteration count exceeds the maximum allowed iterations or the highest acquisition score among the candidate samples falls below a predefined threshold, the algorithm is terminated. If neither condition is met, the process continues with the selection and labeling of new samples.

3.3.6 Selected Samples Update. In this step, we select the top 1% of candidate samples with the highest uncertainty, label them, and add them to the pool of selected samples. These updated samples are then normalized to ensure consistency in data format and scale. Following normalization, the surrogate model is retrained, referring back to step 3.3.2, to incorporate the newly labeled data, thereby enhancing the model's accuracy and reliability.

This algorithmic workflow harnesses the power of GPR combined with AL to provide a state-of-the-art approach for standard cell characterization. The methodology not only achieves high accuracy in waveform prediction but also optimizes the computational resources and time required for simulations.

3.4 Acquisition by Variational Analysis

To evaluate the uncertainty of all candidate samples, we compute the uncertainty of each sample by using the acquisition function (Eq. 5) to evaluate the uncertainty associated with each prediction made by the GPR models. By selecting the top 1% of samples with the highest acquisition scores for retraining and iterating through this process several times, the model achieves significantly improved accuracy.

We define the uncertainty in the distance between the converted voltage waveform from the predicted current waveform of the i -th sample and the simulated voltage waveform as the Acquisition Function. Eq. 5 quantifies how uncertainty in the GP model's predictions at different time or current points contributes to the overall uncertainty in the i -th sample. By multiplying each predicted value's uncertainty with the corresponding gradient and summing these products, we can derive the sample's overall uncertainty. This approach is used to iteratively assess and refine the model's performance.

$$A^{(i)} = \text{Var} \left[L^{(i)} \right] \approx \sum_{j=0}^{n-1} \left(\nabla_{\hat{t}_j} L^{(i)} \right)^2 \text{Var}(t_j) + \sum_{j=0}^{n-1} \left(\nabla_{\hat{i}_j} L^{(i)} \right)^2 \text{Var}(i_j) \quad (5)$$

Here the co-variances between statistical moments are zeros. In the i -th sample, the gradient $\nabla_{\hat{t}_j} L^{(i)}$ or $\nabla_{\hat{i}_j} L^{(i)}$ indicates how sensitive the loss is to small changes in the time point t_j or current point i_j , $j < n$. In 3.3.1, we uniformly extend all time and current data to a consistent length of n points through linear interpolation. This sensitivity is then weighted by the variance of the prediction

at that time or current point, reflecting the contribution of each time or current point's uncertainty to the overall uncertainty of the loss.

In the GPR models, our objective is to estimate the uncertainty of the entire sample based on the uncertainty of each predicted value. To achieve this, we integrate perturbation theory into variational analysis to derive the Root Mean Square Error (RMSE) between the predicted voltage waveform and the simulated waveform concerning a specific predicted value. Using \hat{t}_0 as an example, where \hat{t}_0 represents the predicted initial time point of the voltage waveform and serves as the initial reference for prediction accuracy analysis, the process involves a detailed interpolation procedure.

When calculating the gradients of $L^{(i)}$ with respect to each predicted time point, such as \hat{t}_0, \hat{t}_1 , and so forth, both the predicted waveform and the waveform at a time δ added to the specific time point undergo an interpolation process. This interpolation ensures that both waveforms are aligned over the same $n + 1$ time points, facilitating the calculation of the RMSE across these corresponding voltage values.

Conversely, for gradients with respect to each predicted current value, the process simplifies as the time points for the predicted waveform and the waveform after a change δ in the current value remain consistent. Since the time points do not vary, the RMSE can be directly computed using the voltage values corresponding to these n consistent time points.

The gradient of $L^{(i)}$ with respect to \hat{t}_0 is expressed in Eq 6. Since the simulated voltage waveforms of the candidate samples are not available, we employ an approximation to avoid direct computation with the unknown $V^{(i)*}$. Similarly, the gradients of L with respect to each predicted time point, such as \hat{t}_0, \hat{t}_1 , and so forth, and the corresponding currents can be calculated using the same method.

$$\begin{aligned} \nabla_{\hat{t}_0} L^{(i)} &= \lim_{\delta \rightarrow 0} \frac{1}{\delta} \left[\text{RMSE} \left(V^{(i)}(\hat{t}_0 + \delta) - V^{(i)*} \right) - \text{RMSE} \left(V^{(i)}(\hat{t}_0) - V^{(i)*} \right) \right] \\ &\approx \lim_{\delta \rightarrow 0} \frac{1}{\delta} \left[\text{RMSE} \left(V^{(i)}(\hat{t}_0 + \delta) - V^{(i)}(\hat{t}_0) \right) \right] \end{aligned} \quad (6)$$

4 EXPERIMENTS RESULTS AND DISCUSSION

4.1 Experiment Setup

The proposed cell characterization framework for CCS model is implemented in PyTorch on a Linux machine with NVIDIA 3090 GPU and 8-core Intel Xeon 6348 CPU. It was validated with TSMC 22nm process for 57 cells with different functions and driving strengths shown in Table I under nine PVT corners. In this work, the commercial tool *Liberate* was utilized to generate the training data and the baseline for comparison. The validated nine PVT corners cover the voltages between 0.8V and 0.88V and the temperatures including 0°C and 25°C.

4.2 Verification of Acquisition Function Settings

To assess the accuracy of the settings of the Acquisition Function, we initially applied a falling input on the timing arc of INV X1, which triggered a rising output. Fig. 2 demonstrates the iterative

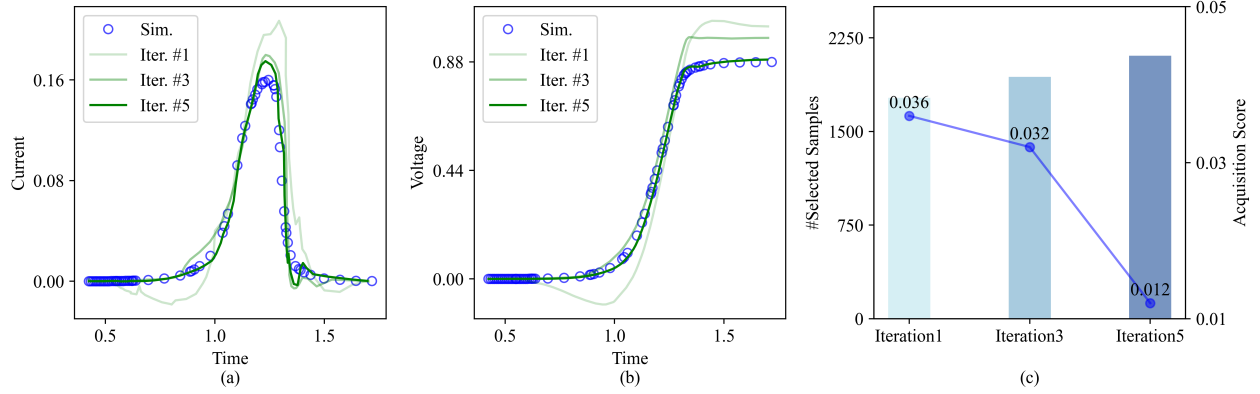


Figure 2: Iterative Process in Waveform Estimation for INV X12 Cell at TT corner, 0.88v, 0°C . (a)Current Waveform Variation. (b)Voltage Waveform Variation. (c)Acquisition Score and Selected Samples Trends.

Table 1: Standard Cell for Validation

Cell Type	Drive Strengths
INV	X2, X3, X4, X6, X8, X9, X12, X15, X16, X18, X20, X21, X24
AN2	X1, X2, X4, X6, X8, X16
ND2, NR2	X0, X1, X2, X3, X4, X6, X8, X16
OR2, AOI21	X0, X1, X2, X4, X6, X8, X16
XOR2, AO21	X0, X1, X2, X4

refinement of the predicted output current waveform. Fig. 2(a) illustrates the evolution of the current waveform throughout the iterations, showing the predicted current waveform progressively converging towards the simulated current waveform as the number of iterations increases. Fig. 2(b) displays the corresponding changes in the voltage waveform during the iterations, with the predicted voltage waveform gradually aligning more closely with the simulated voltage waveform, nearly matching it by the fifth iteration. Fig. 2(c) presents the dynamics in the number of Selected Samples and the variations in the Acquisition Score throughout the iterations. Each iteration adds only 1% more samples to the Selected Samples, leading to only a modest increase in their total number, which facilitates a rapid decrease in the Acquisition Score. Thus, the effectiveness of the Acquisition Function is confirmed, verifying that a lower Acquisition Score corresponds to a predicted waveform that more closely resembles the waveform derived from HSPICE simulations.

4.3 Delay Prediction Accuracy Comparison

To demonstrate the accuracy of our proposed model, we tested it on 57 standard cells under nine PVT corners. In the identical PVT corners, the prediction accuracy of our proposed framework for standard cells is compared with prior works [11, 13] as shown in Table 2 in terms of mean absolute error (MAE) and mean absolute percentage error (MAPE). Our method achieves an average MAE of 2.05 ps and a average MAPE of 2.27% across all cells and PVT

corners, which represents a 6.43× and 4.49× improvement in precision over the Ridge Regression method [11] and CSM-NN method [13]. These enhancements not only demonstrate our framework’s superior accuracy but also underscore its robustness and reliability in handling complex variability across different conditions.

Table 2: Comparison of Delay Accuracy. Unit: ps

Cell Type	Ridge Regression[11]	CSM-NN [13]	Ours
INV	24.64 (24.18%)	15.28 (15.00%)	2.92 (2.87%)
AN2	6.11 (6.42%)	4.36 (4.58%)	1.58 (1.66%)
ND2	20.45 (21.76%)	12.47 (13.27%)	2.55 (2.71%)
OR2	6.53 (6.41%)	5.55 (5.44%)	1.22 (1.19%)
NR2	19.00 (22.18%)	13.46 (15.71%)	2.64 (3.08%)
AO21	4.32 (6.37%)	2.48 (3.66%)	1.33 (1.97%)
AOI21	18.76 (21.74%)	16.08 (18.63%)	2.57 (2.98%)
XOR2	5.72 (6.21%)	3.95 (4.28%)	1.57 (1.70%)
Ave.	13.19 (14.41%)	9.20 (10.07%)	2.05 (2.27%)
Norm.	6.43×	4.49×	1.00×

4.4 Computational and Storage Overhead Comparison

The computational overhead is analyzed and compared in Table 3 and Table 4 in terms of the number of SPICE simulation and runtime respectively, which is occupied to achieve the corresponding prediction accuracy of each method shown in Table 2.

The numbers of SPICE simulations in Table 3 include that for each type of cell of all driving strengths under all PVT corners. It can be seen that during the training of Ridge Regression model [11] and CSM-NN model[13], 80% and 30% samples are randomly selected for each cell respectively by taking the number of SPICE simulations required in commercial tool as baseline. In contrast, the number of simulations for selected samples is adaptively determined for each cell according to the uncertainty quantified by acquisition score,

which are less than 30% for all validated cells with the average ratio of 27%.

In Table 4, the runtime for the proposed characterization framework is compared with the simulation time occupied by traditional commercial tool, which consist of the simulation time for selected samples and the training time for GPR models. It can be seen from Table 4 that the simulation and training time are respectively 26.9% and 17.5% in average compared to that of traditional characterization method, accounting for 44.4% in total. Moreover, the required time for this work further decreases with the increase of cell complexity, which is as low as 23% for AO21 and NR2 cell.

Table 3: Comparison of The Number of SPICE Simulation

Cell Type	Tool	Ridge Regression[11]	CSM-NN [13]	Ours
INV	8424	6739	2527	2527 (30%)
AN2	7776	6221	2333	2022 (26%)
ND2	10368	8294	3110	2903 (28%)
OR2	10368	8294	3110	2799 (27%)
NR2	10368	8294	3110	2385 (23%)
AO21	12960	10368	3888	2981 (23%)
AOI21	22680	18144	6804	6804 (30%)
XOR2	10368	8294	3110	2592 (25%)
Ave.*	100%	80%	30%	27%

* Percentage of the number of simulations for training by taking that for commercial tool as baseline.

Table 4: Runtime Comparison (s)

Cell Type	Tool	Ours		
		SPICE	Train	Total
INV	144.7	42.1 (29.1%)	87.5 (60.5%)	129.6 (92.3%)
AN2	210.7	53.8 (25.5%)	52.5 (24.9%)	106.3 (51.4%)
ND2	246.1	67.4 (27.4%)	70.0 (28.4%)	137.4 (57.1%)
OR2	233.8	61.7 (26.4%)	61.3 (26.2%)	123.0 (53.8%)
NR2	248.9	56.1 (22.5%)	26.3 (10.5%)	82.3 (33.8%)
AO21	257.7	57.8 (22.4%)	26.3 (10.2%)	84.0 (33.4%)
AOI21	1008.2	299.1 (29.7%)	87.5 (8.7%)	386.6 (38.8%)
XOR2	243.8	59.6 (24.5%)	43.8 (17.9%)	103.4 (43.3%)
Ave.	100.0%	26.9%	17.5%	44.4%

Fig. 3 demonstrates the required storage for each cell with this work and traditional library format. In traditional, the points of current waveform for specific function of cell are stored as lookup table (LUT) for each PVT corners and driving strengths, suffering from tremendous storage overhead without the consideration of correlation among these conditions. With the proposed framework, the GPR models are utilized to predict current and time values based on input features. This approach enables efficient inference with trivial computational cost. As compared in Fig. 3, the reduction of storage ranges from 3.4× to 19.5× for all validated cells, which is highly related to the number of PVT corners and driving strengths.

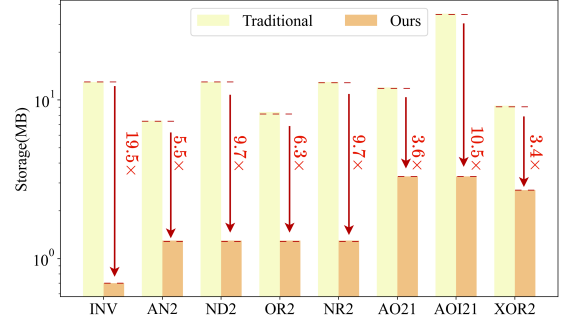


Figure 3: Comparison of storage overhead for CCS model.

Since 11 driving strengths of INV cell are validated in this work, as can be seen in Table 1, it achieves the maximum storage saving.

5 CONCLUSION

In this study, we introduced GPR models with AL that efficiently and accurately characterizes standard cells using the composite current source model. Our model demonstrated superior accuracy, achieving an average absolute error of 2.05 ps and a relative error of 2.27%. Compared to commercial tools, our model requires only an average of 27% of the simulations, significantly reducing the number of SPICE simulation. Furthermore, the model required drastically less storage—up to 19.5 times less than that required by commercial tools. This innovative approach significantly outperforms existing methods and commercial tools in terms of precision, speed, and storage costs.

REFERENCES

- [1] I. K. Rachit and M. S. Bhat. Autolibgen: An open source tool for standard cell library characterization at 65nm technology. In *International Conference on Electronic Design*, pages 1–6, 2008.
- [2] Ratnakar Goyal and Naresh Kumar. Current based delay models: A must for nanometer timing. In *Cadence Live Conference (CDNLive)*, pages 1–8, 2005.
- [3] Dimitrios Garyfallou, Stavros Simoglou, Nikolaos Sketopoulos, Charalampos Antoniadis, Christos P. Sotiriou, Nestor Evmorfopoulos, and George Stamoulis. Gate delay estimation with library compatible current source models and effective capacitance. *IEEE Transactions on Very Large Scale Integration (VLSI) Systems*, pages 962–972, 2021.
- [4] Waseem Raslan and Yehea Ismail. Deep learning autoencoder-based compression for current source model waveforms. In *IEEE International Conference on Electronics, Circuits, and Systems (ICECS)*, pages 1–6, 2021.
- [5] Dimitrios Garyfallou, Anastasis Vagenas, Charalampos Antoniadis, Yehia Masoud, and George Stamoulis. Leveraging machine learning for gate-level timing estimation using current source models and effective capacitance. In *Proceedings of the Great Lakes Symposium on VLSI 2022*, pages 77–83, 2022.
- [6] Siemens. Addressing library characterization and verification challenges using ml. pages 4–6, 2022.
- [7] Synopsys. CCS timing library characterization guidelines, version 3.4. 2016.
- [8] Safar Hatami, Peter Feldmann, Soroush Abbaspour, and Massoud Pedram. Efficient compression and handling of current source model library waveforms. In *Design, Automation & Test in Europe Conference & Exhibition*, pages 1178–1183, 2009.
- [9] Eunice Naswali, Namhoon Kim, and Pravin Chandran. Fast and accurate library generation leveraging deep learning for ocv modelling. In *International Symposium on Quality Electronic Design (ISQED)*, pages 349–354, 2021.
- [10] Eunice Naswali, Adalberto Claudio Quiros, and Pravin Chandran. Dnnlibgen: Deep neural network based fast library generator. In *International Conference on Electronics, Circuits and Systems (ICECS)*, pages 574–577, 2019.

- [11] Florian Klemme and Hussam Amrouch. Machine learning for on-the-fly reliability-aware cell library characterization. *IEEE Transactions on Circuits and Systems I: Regular Papers*, pages 2569–2579, 2021.
- [12] Seyed Milad Ebrahimipour, Behnam Ghavami, Hamid Mousavi, Mohsen Raji, Zhenman Fang, and Lesley Shannon. Aadam: A fast, accurate, and versatile aging-aware cell library delay model using feed-forward neural network. In *Proceedings of the 39th International Conference on Computer-Aided Design*, pages 1–9, 2020.
- [13] Mohammad Saeed Abrishami, Massoud Pedram, and Shahin Nazarian. Csm-nn: Current source model based logic circuit simulation - a neural network approach. In *International Conference on Computer Design (ICCD)*, pages 393–400, 2019.
- [14] Yufei Chen, Xiao Dong, Wei-Kai Shih, and Cheng Zhuo. Unleashing the potential of machine learning: Harnessing the dynamics of supply noise for timing sign-off. In *IEEE/ACM International Conference on Computer Aided Design (ICCAD)*, pages 1–6, 2023.
- [15] Junzhuo Zhou, Ting-Jung Lin, Haoxuan Xia, Li Huang, Wei Xing, and Lei He. LVFGGen: Efficient Liberty Variation Format (LVF) Generation Using Variational Analysis and Active Learning. In *Proceedings of the 2025 International Symposium on Physical Design*, pages 182–190, 2025.
- [16] Kevin P. Murphy. *Machine Learning: A Probabilistic Perspective*. The MIT Press, 2012.
- [17] Charu C. Aggarwal, Xiangnan Kong, Quanquan Gu, Jiawei Han, and Philip S. Yu. *Active Learning: A Survey*, chapter 22, pages 572–605. Chapman and Hall/CRC Press, 2014.
- [18] Dongrui Wu. Pool-based sequential active learning for regression. *IEEE Transactions on Neural Networks and Learning Systems*, pages 1348–1359, 2019.